Sādhanā Vol. 42, No. 5, May 2017, pp. 795–803
DOI 10.1007/s12046-017-0641-9

Mechanical and fracture properties of a self-compacting version of CARDIFRC Mix II

B S AL-AZZAWI and B L KARIHALOO*

School of Engineering, Cardiff University, Cardiff, UK
e-mail: KarihalooB@Cardiff.ac.uk

MS received 5 May 2016; revised 11 November 2016; accepted 25 November 2016

Abstract. CARDIFRC is the trade name of two main groups of ultra-high performance fibre-reinforced concrete mixes – Mixes I and II – differing primarily in the maximum size of quartz sand used (0.6 mm in Mix I, and 2 mm in Mix II). In this paper, the conversion of CARDIFRC Mix II to a self-compacting and industrially competitive ultra-high performance fibre-reinforced concrete (UHPFRC) is described. A full mechanical and fracture characterisation (i.e. size-independent fracture energy and the corresponding bi-linear stress-crack opening relationship) of this UHPFRC is provided.

Keywords. UHPFRC; self-compacting; mechanical properties; toughness; bi-linear stress-crack opening relation.

1. Introduction

Conventional concrete irrespective of its compressive strength has poor tensile and flexural properties and cracks easily (has low toughness), impairing its long-term durability. Attempts have been made in the past, based on ad hoc trial and error tests, to improve the tensile/flexural strengths but this has been accompanied by a reduction in the toughness. The root cause of the intrinsic competition between the strength and toughness is explained by the non-linear theory of fracture [1]. According to this theory the measure of the ductility of a plain or fibre-reinforced concrete mix is its characteristic length [2, 3] $l_{ch} = (EG_F)/(f_t^2)$, where f_t is the tensile strength, G_F the toughness, and E the Young's modulus of the mix. The maximization of l_{ch} of an FRC mix by trial and error enabled researchers to develop a class of ultra-high performance fibre-reinforced cement-based composites (UHPFRC), such as DENSIT [2], RPC and DUCTAL [4–6], characterised by high compressive strength, high tensile/flexural strength, and high toughness.

In the development of CARDIFRC, which also belongs to the class of UHPFRC, the optimization problem of maximizing l_{ch} was solved mathematically. This required a knowledge of the constitutive equations relating the mechanical response parameters (E, f_t, G_F, and compressive strength f_c) to the mix and fibre parameters (water to binder ratio, maximum size of fine aggregate, volume fraction of aggregate, surfactant to water ratio, fibre length, fibre diameter, and fibre volume fraction), collectively called the micro-structural parameters. These were developed in [7] using micro-mechanical principles. The constitutive relations formed the constraints in the optimization problem [8]. The method of the production of CARDIFRC and its mechanical and fracture properties were reported in a series of papers [9–11]. Extensive tests have shown that it has remarkable durability and resistance to thermal cycling and cyclic loading [12, 13]. Computerized tomography imaging and sectioning of specimens have confirmed that the production procedures ensure a remarkably homogeneous mix with a uniform distribution of fibres [11].

Moreover, it improves with age and has self-healing properties because of un-hydrated cement and silica fume. Tests have shown that its toughness increased in 2 years from 20,000 J/m^2 to more than 32,000 J/m^2 [14]. Recent studies [15, 16] have proved that CARDIFRC is very resistant to dynamic loading making it suitable for building critical civil (e.g. nuclear containment vessels) and military infrastructure in order to render it less susceptible to failure under loading by blasts and explosions.

There has been enormous interest in the development of different UHPFRC variants in recent years. The developments until 2007 have been included in the monograph [17]. More recent developments have been reported at the quadrennial RILEM workshops, the most recent one being held in 2015 [18]. In fact, the understanding of the manufacture and testing of UHPFRC has progressed to a state that it can be distilled and simplified for the purposes of engineering design practice. This has resulted in the FIB Model Code 2010 [19]. In the terminology of FIB Model Code 2010 [19], CARDIFRC, together with DENSIT, RPC, and DUCTAL, belongs to the class of UHPFRC that exhibits strain hardening under axial tension. However, the

*For correspondence

rapid development of UHPFRC has not been matched by its industrial uptake. This is not only because of the traditional conservativeness of the construction industry, but also because of the high cost of UHPFRC. Therefore, there is enormous scope for improving the cost-competitiveness of existing UHPFRC.

This paper describes an attempt at improving the cost-competitiveness of CARDIFRC. It summarises the steps taken to produce an industrially competitive version of CARDIFRC. The full mechanical characterisation of the resulting UHPFRC has been provided using standard testing procedures. The fracture properties, however, were obtained using non-standard procedures which made it necessary to provide a brief theoretical background of these procedures.

2. Development of self-compacting UHPFRC from CARDIFRC Mix II

CARDIFRC refers to two main groups of mixes – Mixes I and II – differing primarily in the maximum size of quartz sand used. Both mixes use a large amount of 6 and 13 mm long (0.15 mm diameter) brass-coated steel fibres (total volume fraction 6%). Mix I contains quartz sand up to only 0.6 mm in size, whereas in Mix II the maximum quartz sand size is 2 mm. They were initially developed only for small scale niche applications, e.g. retrofitting of existing concrete structures [12, 20, 21] or jointing of pre-cast concrete elements because of the very high cost of thin brass-coated steel fibres. However, detailed cost analysis in collaboration with a large construction company showed that CARDIFRC can be modified and adapted to make it highly competitive even in a variety of hitherto-unforeseen very large volume applications, e.g. manufacturing pre-cast pre-stressed concrete elements without shear reinforcement for use in structural applications. The advantage of this variant over the competing steel is lower self-weight (which forms a large part of design load), corrosion resistance, and smaller carbon footprint. The development of industrially competitive versions of CARDIFRC in the category of ultra-high performance concrete (UHPFRC) required innovative solutions to many problems. Among these were as follows: (i) reduction of costs by replacing the thin expensive brass-coated steel fibres with only 2.5% by volume of thicker and cheaper steel fibres, 30 mm long and 0.55 mm diameter, with an acceptable reduction in the compressive and flexural strengths (about 30%) but an actual increase (by about 100%) in the toughness; (ii) avoidance of health and environmental hazards by creating self-compacting mixes not requiring noisy vibration and replacing some cement with an industrial waste material, GGBS; and (iii) improvement in the fire resistance to 120 min by using sacrificial polymeric fibres that melt creating channels for the expansion of steam during a fire [22]. The enhanced durability of UHPFRC leads to a longer life and sustainability thereby avoiding structural repair and maintenance costs, and yielding economic, environmental and social benefits. These solutions were first tried on CARDIFRC Mix I [22]. Additional information on the role of fibre content and water to binder ratio on the performance of CARDIFRC Mix I can be found in [23]. Apart from its compressive strength (160 MPa), no other mechanical and fracture properties of this UHPFRC were measured. In this paper, these solutions will be tried on CARDIFRC Mix II. Full mechanical and fracture characterisation of the resulting UHPFRC will be provided. A brief account of this work was presented at a UK conference in 2016 [24].

3. Materials

All constituents used in UHPFRC based on CARDIFRC Mix II were locally available. These included Portland cement Class I 42.5 N, ground-granulated blast furnace slag (GGBS), various grades of quartz sand, Glenium Ace 499 superplasticizer, Elkem Microsilica powder, and 55/30 BG Dramix steel fibres with crimped ends (30 mm long and 0.55 mm diameter, aspect ratio 55). No sacrificial polymeric fibres for enhanced fire resistance were used in this mix. In common with the development of self-compacting mixes from parent vibrated mixes, the powder volume was substantially increased while simultaneously the amount of coarser ingredients was slightly decreased. Thus, 36.4% of cement in the original CARDIFRC Mix II was replaced with GGBS to increase the powder volume and reduce the carbon footprint, while the total amount of quartz sands was reduced by 4.8%. The larger powder content in the self-compacting version required a higher dosage of superplasticizer for attaining the necessary flow-ability (SP/water 0.41 as opposed of 0.37 in the original vibrated CARDIFRC Mix II). The mix proportions are given in table 1.

Table 1. Mix constituents of the self-compacting UHPFRC version of CARDIFRC Mix II (kg/m^3).

Constituent	Dosage (kg/m^3)
Cement	450.3 (744)
Silica fume	169.5 (178)
GGBS	258.0 (0)
Quartz sand:	
9–300 μm	158.0 (166)
0.212–1 mm	318.9 (335)
1–2 mm	639.7 (672)
Water	141.8 (149)
Superplasticizer (SP)	58.5 (55)
Fibres: 30 mm Dramix (vol. 2.5%)	195.0
Water/cement	0.20 (0.20)
Water/binder	0.16 (0.16)
SP/water	0.41 (0.37)
Slump flow spread (mm)	705
t_{500} (s)	2.73

For comparison, the mix proportions of the original vibrated CARDIFRC Mix II are shown in parenthesis in the table.

3.1 *Self-compacting mix preparation*

The mix was prepared in a pan mixer. The volume of a batch was calculated based on the required cube, cylinder and beam test specimens with an allowance for at least four slump flow tests and for some wastage. The mixing procedure recommended by Benson and Karihaloo [9] was followed by adding the finest constituent micro-silica to the coarsest (1–2 mm quartz sand) and mixing them for 2 min. This was followed by the addition of the next coarsest constituent (0.212–1 mm quartz sand) and the next finest constituent (GGBS) and mixing for a further 2 min. Finally, the next coarsest constituent (9–300 μm quartz sand) and the next finest (cement) were added and mixed for a further 2 min. The dry mix was fluidised by a mixture of water and two-thirds of the total superplasticizer (the same amount as in the original CARDIFRC Mix II) in several steps as follows: One-half of the water–superplasticizer mixture was added to the dry mix and mixed for 2 min, followed by one-half of the remaining mixture and mixing. This process of progressive halving of the fluid mixture and mixing was continued until the entire fluid mixture was added. Then the 30 mm long fibres were added. These fibres are supplied by the manufacturer in small packages of about 50 fibres lightly glued together by water-soluble glue. They were scattered slowly and evenly into the rotating pan mixer by hand to avoid their clumping in the mix. Lastly, the remaining one-third of the superplasticizer was added and mixed for 2 min.

3.2 *Slump flow test*

Before transferring the wet fibre-reinforced mix into the slump cone, the mix was visually inspected to estimate its flow-ability. If it appeared to be stiff, additional superplasticiser was added and mixed again for 2 min. It was then transferred into the slump cone and the test was performed according to BS EN 12350-8 [25]. If it did not meet the flow-ability criterion, namely that the time to reach the flow diameter of 500 mm (t_{500}) is less than 3 s, additional superplasticizer was added to the remaining mix in the pan mixer, and the test repeated. This time was chosen somewhat arbitrarily to be near the boundary, $t_{500} \leq 2$ s, between the two viscosity classes (VS1 and VS2) according to BS EN 206-9 [26]. Two to three trials were needed to meet the flow-ability criterion. The slump flow spread of the self-compacting mix that met the target t_{500} is shown in figure 1. The mix proportions of the UHPFRC based on CARDIFRC Mix II are given in table 1.

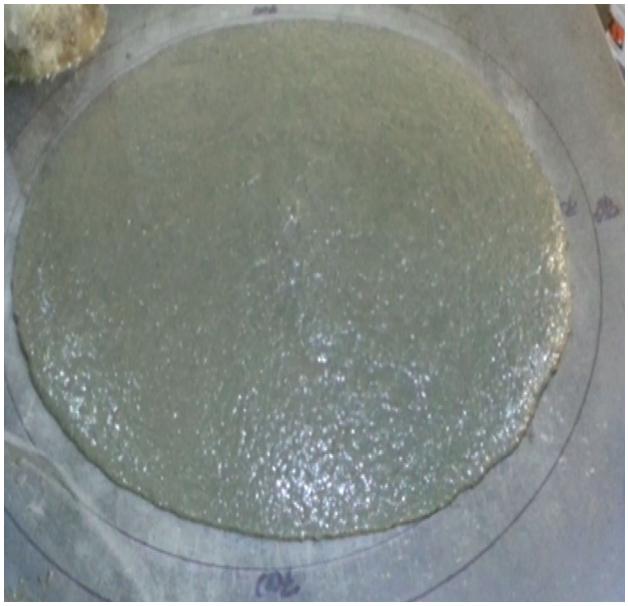

Figure 1. Slump flow spread of UHPFRC based on CARDIFRC Mix II.

3.3 *Specimen curing*

The mix was then cast into standard cube (100 mm), cylinder (100 × 200 mm) and beam (100 × 100 × 500 mm) moulds. The specimens were de-moulded after 24 h and placed in a water tank. The water was heated slowly to 90°C in 24 h to avoid thermal shock, and the specimens were cured at this elevated temperature for 7 days. The temperature was then reduced gradually to ambient condition within 24 h. The specimens were taken out of the water tank and air dried prior to testing. It should however be noted that tests have shown [20] that mixes can also be cured in water at ambient temperature for 28 days with no noticeable difference in the mechanical properties.

4. Mechanical properties

Compression tests were carried out on cube specimens according to BS EN 12390-3 [27], whereas split tensile tests were performed on cylindrical specimens according to BS EN 12390-6 [28]. In addition, the modulus of elasticity was measured on a cylindrical specimen according to BS 1881-121 [29] and the modulus of rupture of beam specimens was determined according to BS 1881-118 [30]. Table 2 shows the mechanical properties of the UHPFRC, together with the coefficient of variation (CoV in %).

As expected, the compressive strength, the tensile splitting strength and the modulus of rupture of the UHPFRC are inferior to those of the CARDIFRC Mix II [10] because of the absence of thin short (6 mm) brass-coated steel fibres (4.5% by volume). The modulus of elasticity, on the other hand, is only marginally reduced.

Table 2. Mechanical properties of the self-compacting UHPFRC version of CARDIFRC Mix II.

Compressive strength (MPa)	Split cylinder strength (MPa)	Modulus of rupture (MPa)	Modulus of elasticity (GPa)
148.0 (4.5%)	18.5 (6.0%)	20.0 (0.7%)	45.2 (0.2%)

5. Fracture properties

5.1 *Specific fracture energy – theoretical background*

Not only the superior mechanical properties of UHPFRC (table 2) are of practical interest, but even more important is their superior fracture resistance. It is quantified by the energy consumed per unit area of crack surface, also called the specific fracture energy. No standard test exists for its measurement, but RILEM-50FMC [31] has recommended a method based on the work-of-fracture, e.g. the area under the load-mid-span deflection curve of a notched beam loaded in three-point bending. According to the RILEM recommendation, the specific fracture energy G_f is the average energy given by dividing the total work-of-fracture by the projected fracture area (i.e. area of initially un-cracked ligament) using a pre-cracked (notched) specimen. This method is equally applicable to UHPFRC, despite the fact that the test may have to be terminated before the the tail part of the load–deflection plot has been registered, i.e. the specimen has completely fractured, because the fibre bridging provides substantial residual load bearing capacity up to very large crack openings. In this situation, the work-of-fracture is corrected using the procedure described in [32]. Alternatively, the area under the load–deflection curve up to particular deflection levels may be expressed as a multiple of the area up to the limit of proportionality to determine the so-called toughness indices of UHPFRC, designated I_5, I_{10}, etc. where the subscript denotes the multiple of the area. A detailed review of the many variations of toughness index approach can be found in the monograph [17].

The specific fracture energy, G_f, is known to vary with the size and shape of the test specimen. The cause of this variability is explained in [33], namely that the local specific fracture energy is not constant along the crack path in a test specimen. It decreases as the crack grows along the un-notched ligament with the rate of decrease picking up speed as the crack approaches the back, stress-free boundary of the specimen. For this reason, the Hu-Wittmann model is also called the boundary effect model [34, 35]. They proposed a bi-linear approximation for the local fracture energy variation (g_f)along the crack path (figure 2) with the intersection of the two asymptotes defining a transition ligament size (a_l) and used this approximation to derive relations between the measured size-dependent fracture energy (G_f), the transition length (a_l) and the size-independent fracture energy (G_F).

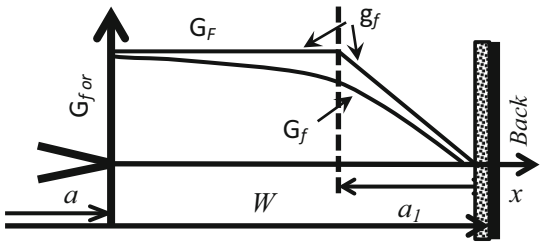

Figure 2. Bi-linear local fracture energy $G_f\left(\frac{a}{W}\right)$ variation along the un-notched ligament of a notched specimen.

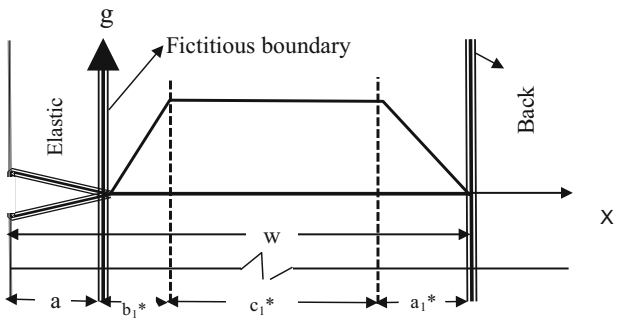

Figure 3. Tri-linear approximation of local fracture energy gf variation over the un-notched ligament length [39].

The values of G_F and $a_l$of a concrete mix are obtained from these relations once the size-dependent specific fracture energy (G_f) of the mix has been measured on specimens of different sizes and several notch to depth ratios using a least squares method on the over-determined system of equations. However, a simplification of this boundary effect method was proposed in [36], requiring only testing of notched beam specimens of identical size (beam height W, notch depth a) by the RILEM work-of-fracture method. One half of the specimens have a shallow starter notch (a/W = 0.1), while the other half have a deep starter notch (a/W = 0.6), straddling the expected transition length ratio a_l/W. This simplification reduces the number of test specimens and avoids the use of least squares minimisation. It was validated in [37] on a series of available test results. It has been shown in [38] that although the measured values of G_f depend on W and a/W, the above procedure indeed leads to a value of G_F that is essentially independent of the specimen size and relative notch depth.

In recent works, a tri-linear approximation of the local fracture energy along the unbroken ligament was proposed in [39–41]. As has been shown by acoustic emission data, the tri-linear approximation is closer to how the local fracture energy varies as the crack grows from a notched specimen [39]. The local fracture energy (G_f) first rises from the fictitious boundary (notch tip), then remains nearly constant G_F, before reducing again as the crack approaches the stress-free back face boundary, figure 3. It has been found in [42] that the bi-linear and tri-linear approximations result in

nearly the same values of the size-independent specific fracture energy(G_F). For this reason, the simplified boundary effect method introduced in [36] based on the bi-linear approximation [33] will be used below.

5.2 *Test results*

Six prisms 100 × 100 × 500 mm were cast with the self-compacting UHPFRC. After curing, three prisms were notched to a depth of 10 mm and the remaining three to a depth of 60 mm using a diamond saw (width approximately 2 mm). They were tested in three-point bending over a loaded span of 400 mm. The test was controlled first by a feedback signal from a crack mouth opening displacement (CMOD) gauge until the gauge reached its limit (around 3.5 mm), where after the control switched to mid-point displacement control. The load–CMOD was recorded until the gauge reached its limit, but the load-mid-point displacement continued to be recorded until the displacement reached 30 mm. The load had still not dropped to zero. The area under the load–deflection plot was therefore corrected to account for the unrecorded work-of-fracture using the procedure described in [32]. The total work-of-fracture was divided by the projected fracture area (i.e. area of initially un-cracked ligament) of the notched specimen to calculate the specific fracture energy $G_f(a/W)$ corresponding to a/W = 0.1 and 0.6. Finally, the size-independent specific fracture energy G_F and a_l were determined using the appropriate relations of the boundary effect model [33]. The values are reported in table 3. The size-independent specific fracture energy is 36,300 N/m compared to about 20,000 N/m for the original vibrated Mix II measured in axial tension. The increase in primarily due to the use of a larger volume (2.5%) of longer (30 mm) fibres in the UHPFRC compared with the CARDIFRC Mix II in which only 1.5% by volume of 13 mm long fibres was used.

Table 3. Mean size-dependent fracture energies for a/W = 0.1 and 0.6 and size-independent specific fracture energy of UHPFRC version of CARDIFRC Mix II (bi-linear model).

Notch (mm)	Mean G_f (N/m)	a_l (mm)	G_F (N/m)
10	30,190	30.3	36,300
60	22,600		

5.3 *Stress-crack opening relation – theoretical background*

The analysis of cracked concrete structures using the fictitious crack model [1, 43] requires not just the size-independent fracture energy of the concrete G_F, but also its softening behaviour. In the fictitious crack model (FCM) it is assumed that after crack initiation, stresses may be transmitted across the fictitious crack faces. These crack bridging forces are assumed to be a function of the crack opening displacement given by the stress-crack opening relationship. The stress-crack opening relationship of the early FCM was modelled as a linear function which has been found not to capture the essence of the tension softening of concrete. After the initiation of a crack, concrete is known to soften rapidly because of microcracking, but the rate decreases thereafter because of aggregate interlock and other frictional processes, and especially fibre bridging forces. Therefore, to capture the observed tensile/flexural behaviour of fibre-reinforced concrete, the stress-crack opening relationship must be at least a bi-linear function [44]. The area under this bi-linear diagram is equal to G_F.

It was proposed in [45] that the flexural failure of concrete beams may be modelled by the development of a fictitious crack in a central segment with a width proportional to the beam depth. They treated this segment as a cracked hinge (figure 4) with a linear stress-crack opening relationship.

The bending failure was modelled in [44] in the same way, using a bi-linear stress-crack opening relationship

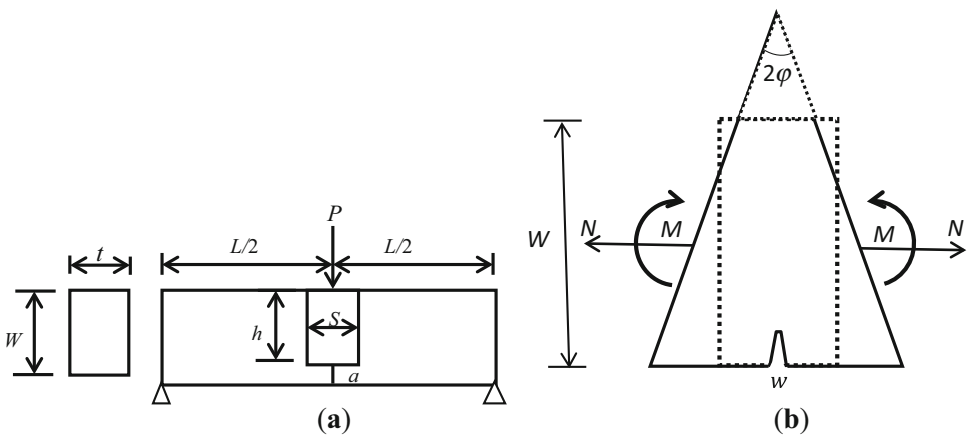

Figure 4. (**a**) Loading and geometry of cracked hinge model and (**b**) deformation of the cracked hinge.

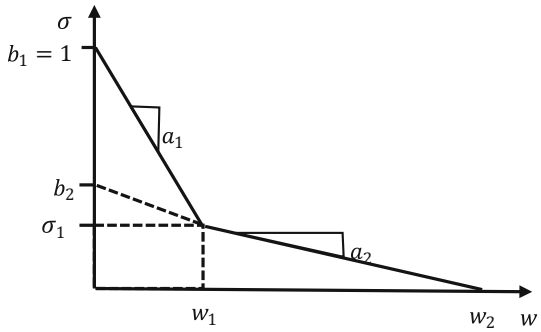

Figure 5. Bi-linear stress-crack opening diagram.

instead. The isolation of the segment of a beam near the propagating crack and its modelling as a short beam segment subjected to a bending moment and a normal force is the basic concept of the non-linear cracked hinge model [44], (figure 4a, b). This is a generic model applicable to both plain and fibre-reinforced concrete.

In the non-linear hinge model the crack is viewed as a local change in the overall stress and strain field. This change is assumed to vanish outside a certain band of width s (figure 4a). Thus, outside of this band the structural element is modelled using the elastic beam theory. This inverse approach for identifying the material stress-crack opening relation is far superior to the approximate inverse approach proposed in FIB Model Code [19] which is intended for engineering practice.

The constitutive relationship for each segment inside the hinge is assumed to be linear elastic up to the peak load (phase 0), while the cracked state is approximated by a bi-linear softening curve as shown in figure 5.

The non-linear cracked hinge is incorporated into the notched beam at mid-span, and the load–deflection and load–CMOD relationships of the beam are established depending on the position of the fictitious crack along the depth of the beam. The axial load and bending moment (figure 4) are related to the hinge rotation in three phases depending on the position of the fictitious crack ahead of the real notch: (i) the fictitious crack is entirely on the first branch of the bi-linear softening diagram; (ii) it is partly on the first and partly on the second branches; and (iii) it is entirely on the second branch. The full analytical expressions relating the hinge rotation to the bending moment in each of these three phases and in turn to the applied central load on the beam are given in [44].

5.4 *Test results*

The unknown parameters of the bi-linear stress-crack opening diagram, e.g. w_1, w_2, f_t and σ_1/f_t or a_1, a_2, f_t and σ_1/f_t are identified in an inverse manner by minimizing the root mean square error between either the recorded and predicted load–CMOD or the load–deflection diagram at many values of the applied central load. This is generally possible for all plain and conventional fibre-reinforced concrete mixes in which the load–CMOD and load–deflection diagrams can be recorded almost until the load has dropped to zero within the limits of measurement of the CMOD gauge (about 3.5 mm) or LVDT (can be up to 50 mm). For UHPFRC of the strain-hardening type though the inverse identification procedure can be applied only to the load–deflection plot which can be recorded to very large deflection values, but not to the load–CMOD record which is restricted by the range of CMOD gauge to almost only the pre-peak response. Accordingly, the parameters of the bi-linear tension softening diagrams for both notches have been identified using the inverse identification procedure on the load–deflection plots recorded up to a deflection of 30 mm. The parameters so identified are tabulated in table 4 and shown in figure 6. The recorded and predicted load–deflection curves for notch-to-depth ratios 0.1 and 0.6 are shown in figure 7. The error shown in table 4 is obtained by calculating the difference between the measured size-dependent fracture energy (G_f) and that given by the area under the stress-crack opening diagram for each notch depth (figure 5)

$$G_f = \frac{1}{2} f_t \left(w_1 + \frac{\sigma_1}{f_t} w_2 \right). \tag{1}$$

An additional check on the accuracy of the parameters of the bi-linear stress-crack opening relation is provided by predicting the load–CMOD plot and comparing it with the restricted recorded plot. This is done in figure 8 for one notch-to-depth ratio (a/W = 0.1), from which it can be concluded that the identified parameters for this notch-to-depth ratio are accurate.

The assumption that the response of the non-linear hinge is linear elastic up to the peak load implies that the pre-peak non-linear strain-hardening cannot be captured by the hinge

Table 4. Bi-linear tension softening diagram parameters corresponding to $a/W = 0.1$ and 0.6 and the size-independent G_F.

Item	a_1 (mm^{-1})	a_2 (mm^{-1})	b_2	w_1 (mm)	w_2 (mm)	σ_1/f_t	f_t (MPa)	Percentage difference (%)
a/W = 0.6	0.256	0.11	0.63	2.5	5.8	0.36	10.44	5.8
a/W = 0.1	0.16	0.07	0.59	4.55	8.43	0.27	9.54	7.4
G_F	0.18	0.09	0.66	3.76	7.38	0.324	12.02	

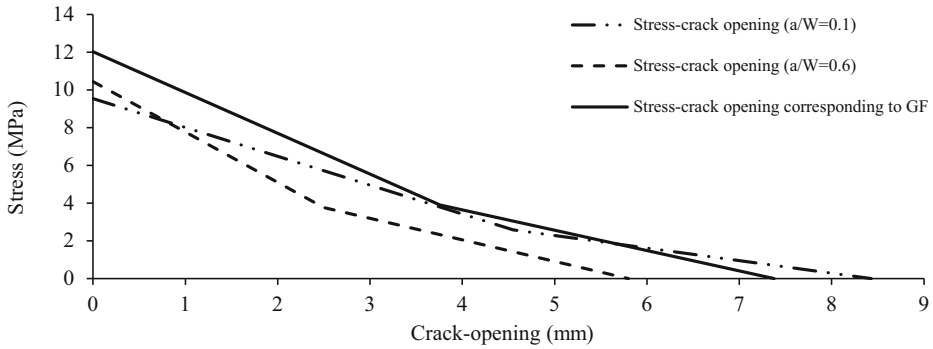

Figure 6. Bi-linear stress-crack opening relationships corresponding to $a/W = 0.6$, 0.1 and G_F.

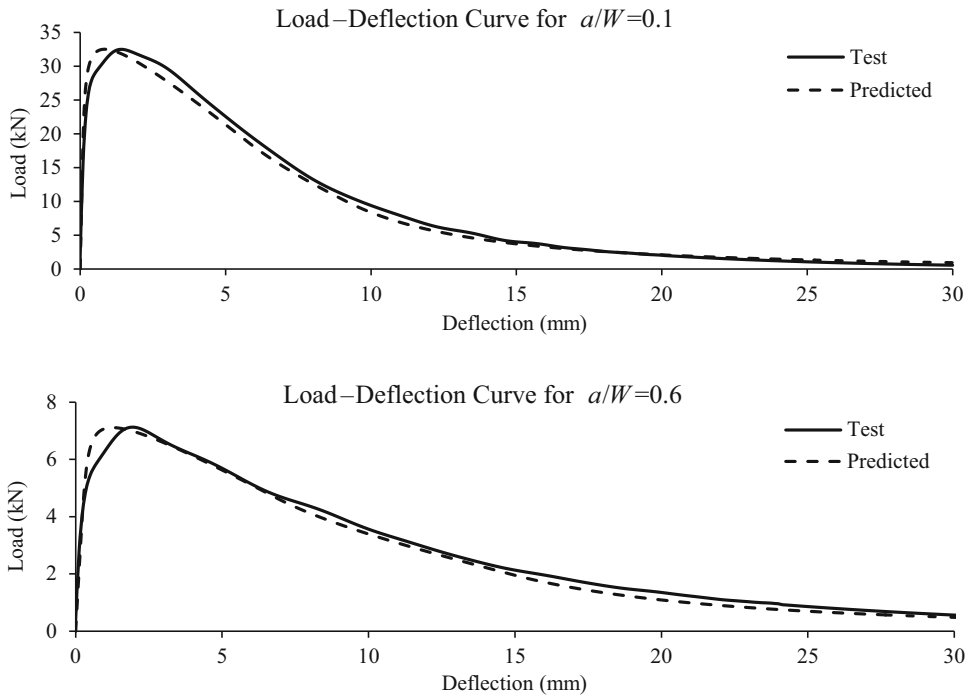

Figure 7. Predicted and recorded load–deflection curves for $a/W = 0.1$ and 0.6.

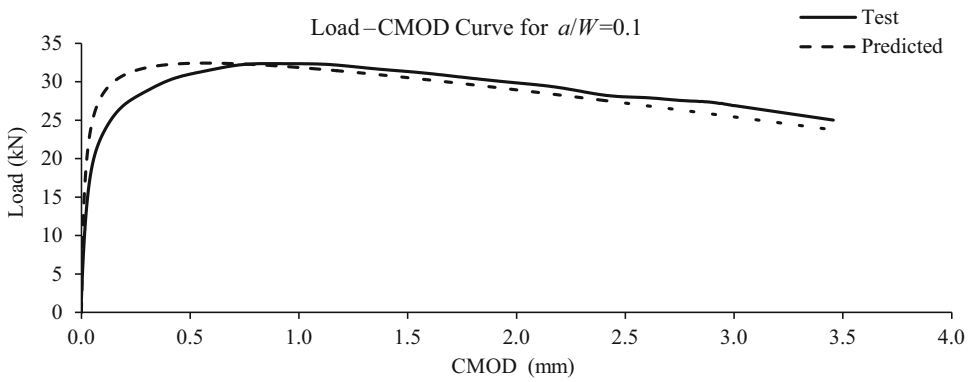

Figure 8. Predicted and recorded load–CMOD curves for a/W= 0.1.

model (figures 7 and 8). This pre-peak non-linearity is known to be a result of diffuse micro-cracking whose density increases as the load is increased from the linear elastic proportional limit to the peak load. It can be captured by considering the effect of micro-cracks on the reduction in the stiffness using the micromechanical formulation described in [46].

The parameters of the tension softening curves obtained using the non-linear hinge model correspond to the measured G_f (0.1) and G_f (0.6), but not to G_F.

A simple method has been proposed in [47] for the determination of the bi-linear softening diagram corresponding to the size-independent G_F of concrete mix by scaling the average parameters of the tension softening diagrams corresponding to the size-dependent fracture energies G_f (0.1) and G_f (0.6) (table 4). This scaling procedure was followed in this work, giving the parameters reported in the last row of table 4. The corresponding tension softening diagram is also shown in figure 7.

It should be mentioned that, as expected, the direct tensile strength of the UHPFRC is less than that of the original CARDIFRC Mix II (12.02 MPa in contrast to 15 MPa). This is because of the absence of short steel fibres (6 mm long, 4.5% by volume) in the UHPFRC.

6. Conclusions

1. A self-compacting UHPFRC based on CARDIFRC Mix II was developed and fully characterised from both the mechanical and fracture points of view. As expected, the resulting UHPFRC has inferior compressive, tensile and flexural strengths than the original CARDIFRC Mix II. This is due to the absence of thin small brass-coated steel fibres (4.5% by volume; 6 mm long) in the UHPFRC. The UHPFRC is, however, much tougher thanks to the use of a larger volume fraction (2.5% against 1.5%) of longer steel fibres (30 mm against 13 mm).
2. An inverse approach based on the non-linear hinge model for crack growth from a pre-existing notch was used to identify the parameters of the bi-linear stress-crack opening relation of the UHPFRC.
3. The load–deflection and load–CMOD curves of notched beams predicted using the bi-linear stress-crack opening relations were shown to be in very good agreement with the recorded experimental results, except in the pre-peak non-linear region.

References

[1] Hillerborg A, Modeer E and Petersson P E 1976 Analysis of crack formation and crack growth in concrete by means of fracture mechanics and finite elements. *Cement Concr. Res.* 6(6): 773–781

[2] Bache H H 1981 *Densified cement ultra-fine particle-based materials*. CBL Report No. 40, Aalborg Portland, Denmark

[3] Karihaloo B L 1995 *Fracture mechanics and structural concrete.* Harlow, Essex: Addison Wesley Longman

[4] Bonneau O, Poulin C, Dugat J, Richard P and Aitcin P C 1996 Reactive powder concretes: from theory to practice. *ACI Int. Concr. Abstr. Portal* 18(4): 47–49

[5] Bonneau O, Lachemi M, Dallaire E, Dugat J and Aitcin P C 1997 Mechanical properties and durability of two industrial reactive powder concretes. *ACI Mater. J.* 94(4): 286–290

[6] Morin V, Cohen Tenoudji F, Feylissoufi A and Richard P 2001 Superplasticizer effects on setting and structuration mechanisms of ultra-high performance concrete. *Cement Concr. Res.* 31(1): 63–71

[7] Karihaloo B L, Wang J and Grzybowski M 1996 Doubly periodic arrays of bridged cracks and short-fibre reinforced cementitious composites. *J. Mech. Phys. Solids* 44(10): 1565–1586

[8] Lange-Kornbak D and Karihaloo B L 1996 Design of concrete mixes for minimum brittleness. *J. Adv. Cement-Based Mater.* 3(3–4): 124–132

[9] Benson S D P and Karihaloo B L 2005a CARDIFRC – development and mechanical properties. Part 1: development and workability. *Mag. Concr. Res.* 57(6): 347–352

[10] Benson S D P and Karihaloo B L 2005b CARDIRFC – development and mechanical properties. Part III: uniaxial tensile response and other mechanical properties. *Mag. Concr. Res.* 57(8): 433–443

[11] Benson S D P, Nicolaides D and Karihaloo B L 2005 CARDIFRC – development and mechanical properties. Part II: fibre distribution. *Mag. Concr. Res.* 57(7): 412–432

[12] Farhat F A, Nicolaides D, Kanellopoulos A and Karihaloo B L 2007 CARDIFRC – performance and application to retrofitting. *Eng. Fract. Mech.* 74(1–2): 151–167

[13] Nicolaides D, Kanellopoulos, A D and Karihaloo B L 2010 Fatigue life and self-induced volumetric changes of CARDIFRC. *Mag. Concr. Res*. 62: 679–683

[14] Nicolaides D 2004 *Fracture and fatigue of CARDIFRC*. PhD thesis, Cardiff University, UK

[15] Petrov Y V, Karihaloo B L, Bratov V V and Bragov A M 2012 Multi-scale dynamic fracture model for quasi-brittle materials. *Int. J. Eng. Sci.* 61(December): 3–9

[16] Bragov A M, Karihaloo B L, Petrov Y V, Konstantinov A Y, Lamzin D A, Lomunov A K and Smirnov IV 2013 Dynamic strengths and toughness of an ultra-high performance fibre-reinforced concrete. *Eng. Fract. Mech.* 110(9): 477–488

[17] Bentur A and Mindess S 2007 *Fiber reinforced cementitious composites*, 2nd edn, chapter 6, Taylor and Francis, London

[18] Reinhardt H W, Parra-Montesinos G J and Garrecht H (eds.) 2015 *High-performance fiber reinforced cement composites (HPFRCC7),* RILEM Publ.PRO 94, Fraunhofer IRB Verlag

[19] FIB Bulletin 55: *Model code 2010 fibre-reinforced concrete*, First Complete Draft, volume 1

[20] Karihaloo B L, Alaee F J and Benson S D P 2002 A new technique for retrofitting concrete structures. *Proceedings of the ICE – J. Struct. Build.* 152(4): 309–318

[21] Alaee F J and Karihaloo B L 2003 Retrofitting RC beams with CARDIFRC. *ASCE J. Compos. Constr.* 7(3): 174–186

[22] Karihaloo B L 2011 CARDIFRC – From concept to industrial application. In: Parra Montesinos G J, Reinhardt H W and Naaman A E (eds.) *Proceedings 6th RILEM Workshop on High Performance Fiber Reinforced Cement Composites (HPFRCC6)*. RILEM Publications S.A.R.L., France, pp 397–404

[23] Karihaloo B L 2012 Influence of micro-structural parameters and thermal cycling on the properties of CARDIFRC. *Sadhana, Indian Acad. Sci.* 37(1): 125–132

[24] Al-Azzawi B S and Karihaloo B L 2016 Fracture and fatigue of a self-compacting version of CARDIFRC mix II. In: *Proceedings of the 24th UK Conference of the Association for Computational Mechanics in Engineering*, Cardiff University, Cardiff https://acme2016.sciencesconf.org/89958/document

[25] BS EN 12350-8, 2010 *Testing fresh concrete, Part 8: Self-compacting concrete, Slump-flow test*. British Standards Publication

[26] BS EN 206-9 2010 *Concrete, Part 9: Additional rules for self-compacting concrete (SCC)*. British Standards publication

[27] BS EN 12390-3 2009 *Testing hardened concrete, Part 3: Compressive strength of test specimens*. British Standards publication

[28] BS EN 12390-6 2009 *Testing hardened concrete, Part 6: tensile splitting strength of test specimens*. British Standards publication

[29] BS 1881-121 1983 *Method for determination of static modulus of elasticity in compression*. British Standards publication

[30] BS 1881-118 1983 *Method for determination of the modulus of rupture of beam specimens*. British Standards publication

[31] RILEM-50FMC 1985 Determination of the fracture energy of mortar and concrete by means of three-point bend tests on notched beams. *Mater. Struct.* 18(106): 285–290

[32] Elices M, Guinea G V and Planas J 1992 Measurement of the fracture energy using three-point bend tests: Part 3 – influence of cutting the *P-d* tail. *Mater. Struct.* 25: 327–334

[33] Hu X and Wittmann F H 1992 Fracture energy and fracture process zone. *Mater. Struct.* 25(6): 319–326

[34] Duan K, Hu X and Wittmann F H 2003 Boundary effect on concrete fracture and non-constant fracture energy distribution. *Eng. Fract. Mech.* 70: 2257–2268

[35] Duan K, Hu X and Wittmann F H 2007 Size effect on specific fracture energy of concrete. *Eng. Fract. Mech.* 74(1–2): 87–96

[36] Abdalla H M and Karihaloo B L 2003 Determination of size-independent specific fracture energy of concrete from three-point bend and wedge splitting tests. *Mag. Concr. Res.* 55(2): 133–141

[37] Karihaloo B L, Abdalla H M and Imjai T 2003 A simple method for determining the true specific fracture energy of concrete. *Mag. Concr. Res.* 55: 471–481

[38] Hu X and Duan K 2004 Influence of fracture process zone height on fracture energy of concrete. *Cement Concr. Res.* 34(8): 1321–1330

[39] Muralidhara S, Prasad B K R, Eskandari H and Karihaloo B L 2010 Fracture process zone size and true fracture energy of concrete using acoustic emission. *Constr. Build. Mater.* 24(4): 479–486

[40] Muralidhara S, Prasad B K R, Karihaloo B L and Singh R K 2011 Size-independent fracture energy in plain concrete beams using tri-linear model. *Constr. Build. Mater.* 25(7): 3051–3058

[41] Karihaloo B L, Murthy A R and Iyer N R 2013 Determination of size-independent specific fracture energy of concrete mixes by the tri-linear model. *Cement Concr. Res.* 49(July): 82–88

[42] Murthy R A, Karihaloo B L, Iyer N R and Raghu Prasad B K 2013 Determination of size-independent specific fracture energy of concrete mixes by two methods. *Cement Concr. Res.* 50(August): 19–25

[43] Hillerborg A 1980 Analysis of fracture by means of the fictitious crack mode, particularly for fiber-reinforced concrete. *Int. J. Cement Compos.* 2(4): 177–184

[44] Olesen J F 2001 Fictitious crack propagation in fiber-reinforced concrete beams. *ASCE J. Eng. Mech.* 127(3): 272–280

[45] Ulfkjaer J, Krenk S and Brincker R 1995 Analytical model for fictitious crack propagation in concrete beams. *J. Eng. Mech.* 121(1): 7–15

[46] Budiansky B and O'Connell R J 1976 Elastic moduli of a cracked solid. *Int. J. Solids Struct.* 12: 81–97

[47] Abdalla H M and Karihaloo B L 2004 A method for constructing the bilinear tension softening diagram of concrete corresponding to its true fracture energy. *Mag. Concr. Res.* 56(10): 597–604